Carbon 119 (2017) 350–354

Contents lists available at ScienceDirect

Carbon

journal homepage: www.elsevier.com/locate/carbon

Towards the standardization of graphene growth through carbon depletion, refilling and nucleation

Bing Liu [a], Ningning Xuan [a], Kun Ba [a], Xianchong Miao [b], Minbiao Ji [b], Zhengzong Sun [a, c, *]

[a] Department of Chemistry, Fudan University, Shanghai 200433, PR China
[b] Department of Physics, Fudan University, Shanghai 200433, PR China
[c] Department of Chemistry and Shanghai Key Laboratory of Molecular Catalysis and Innovative Materials, Fudan University, Shanghai 200433, PR China

ARTICLE INFO

Article history:
Received 6 February 2017
Received in revised form
13 April 2017
Accepted 22 April 2017
Available online 24 April 2017

ABSTRACT

As the graphene is transforming from a laboratory niche material into a mass-produced industrial commodity, maintaining high quality standard across different chemical vapor deposition (CVD) systems becomes the first priority. In this paper, we investigated the carbon diffusion behavior involving two kinds of annealing gases, which reduced the nucleation density in different rate. Compared to the time-consuming and hazardous high-pressure H_2 annealing, O_2 annealing represents a more efficient route to reduce the nucleation density down to ~10 nuclei cm^{-2} in half an hour. We also proposed a well-defined carbon depletion and refilling mechanism, with which we can precisely gauge the minute carbon concentration inside Cu (less than 10 ppm), and control the nucleation density in a reproducible manner. Moreover, we find that O_2 displays an impressive carbon depletion activity, ~6 order more efficient than H_2. The graphene single crystals' quality was confirmed with Raman spectroscopy and field effect transistor (FET) devices.

1. Introduction

Since 2004, graphene has emerged as the representative two-dimensional (2D) materials with superb physical properties like excellent electrical conductivity, thermal stability and mechanical strength [1–5]. As an important candidate for 2D electronics, a lot of research attention has been casted on its synthesis of large area films and single domain crystals over the past several years [6–9]. CVD-grown graphene films are born polycrystalline with grain boundaries, degrading its electrical performance [10]. Therefore, the single crystal pathway through restricting nucleation density becomes more technically attractive. Fig .1a illustrates how the nucleation density determines the final two forms of products. Low density favors the single crystal pathway. The research of growing graphene single crystals [11–13] flourished right after the first Cu-catalyzed CVD graphene film [6,14]. In 2012, on molten Cu surfaces, ~100-200 μm-sized single crystals were synthesized [15,16]. Later, the size was quickly pushed into millimeter region [17–19]. Tour's group obtained 2.3 mm-sized hexagonal shaped monolayer graphene crystals on electrochemically polished and H_2-annealed Cu substrates [18]. In their report, the importance of long period and high-pressure H_2 treatment was identified as the critical step to reduce the nucleation density. The recent crystal's size was doubled by utilizing intrinsic cupric oxide layer on Cu surface to further reduce the nucleation density [17]. Experimentally, people are getting larger and larger graphene crystals in their own CVD systems with specific growth recipes [20,21]. However, most of the experiments were carried out with their own sets of instruments and gas-introducing steps, therefore ended up with complex results and controversial mechanism, which hurdles the real industrial applications of this material.

In order to elucidate the mechanism of graphene nucleation, we break down the CVD graphene growth into two steps: carbon depletion and refilling. The ideal nucleation condition was featured with a fast and thorough carbon depletion followed with a slow refilling step. The speeds of the depletion and refilling processes can be tuned chemically with controlled H_2 or O_2 flows and the CH_4 partial pressures. The carbon concentration and its diffusion behavior at ~1070 °C were synchronously considered.

2. Experimental

2.1. Single crystal graphene synthesis

A tubular Cu substrate, formed by rolling a piece of electro-

* Corresponding author. Department of Chemistry, Fudan University, Shanghai 200433, PR China.
E-mail address: zhengzong_sun@fudan.edu.cn (Z. Sun).

http://dx.doi.org/10.1016/j.carbon.2017.04.055
0008-6223/

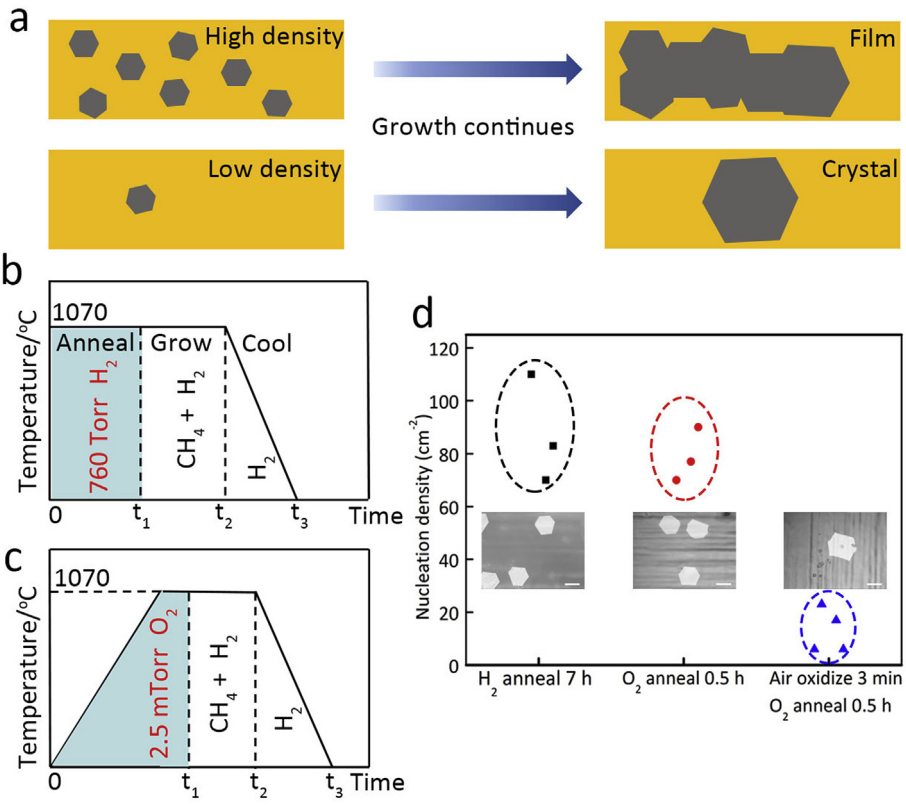

Fig. 1. Graphene nucleation density with H_2-annealing and O_2-annealing methods. (**a**) A schematic illustration showing the difference of high and low nucleation density for film and single crystals. (**b**) Growth with H_2-annealing. (**c**) Growth with O_2-annealing. (**d**) Nucleation density with different annealing methods. The flow rate ratio of H_2/CH_4 during growth is 900:1 and the growth time is 0.5 h. Scale bars: 50 μm in (**d**). (A colour version of this figure can be viewed online.)

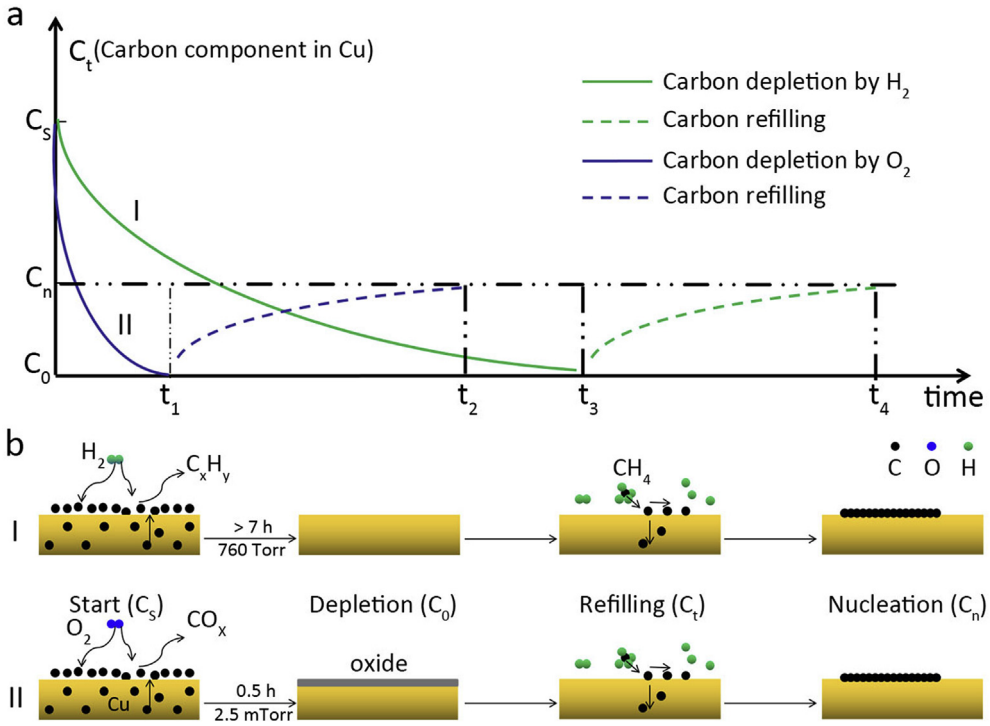

Fig. 2. Carbon diffusion schemes in graphene growth. (**a**) The profiles depicting the time evolution of carbon concentration in Cu (C_t) following the two respective methods. Both purple and green solid curves represent the carbon-depletion steps. Both purple and green dashed lines represent the carbon-refilling stages. The initial carbon concentration in Cu is C_s, varying with different samples. C_0 is the carbon concentration when soluble carbon is thoroughly depleted from Cu. C_n is the carbon concentration when graphene starts to nucleate. (**b**) The schematic illustration depicting possible mechanisms of the two separate methods, H_2 and O_2 annealing, respectively. (A colour version of this figure can be viewed online.)

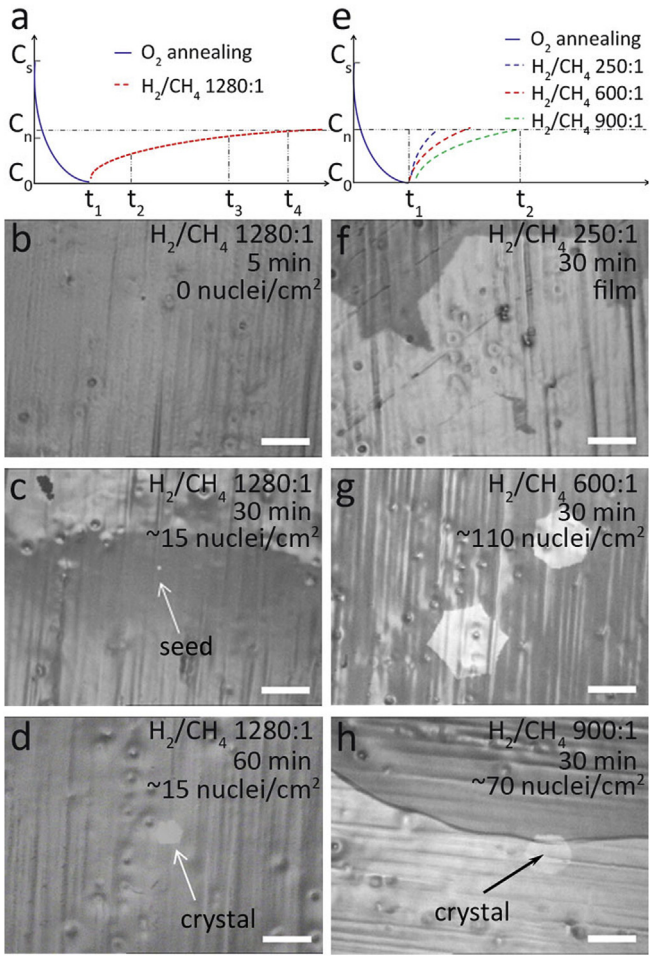

Fig. 3. Graphene nucleation density under varying growth condition. (**a**) The profile depicting the carbon concentration in Cu with fixed H_2/CH_4 ratio ~1280:1 and different growth time. (**b-d**) Representative optical images of the growth results on Cu substrates of different refilling time of 5 min, 30 min and 60 min, respectively. (**e**) The profile depicting the carbon concentration in Cu with different carbon refilling rate. (**f-h**) Representative optical images of growth result on Cu substrates with 30 min growth duration. The H_2/CH_4 ratios are 250:1, 600:1 and 900:1, respectively. Scale bars: 100 μm. (A colour version of this figure can be viewed online.)

chemically polished Cu foil with a glass rod, was adapted to grow single crystals of graphene. This tubular shape can facilitate the Cu vapor to reach equilibrium between evaporation and re-deposition and improve the inner surface's smoothness [19] (Fig. S1). To consistently assess the nucleation density, we only count the crystals grown on the inner surface, as the outer surface works as a shelter and is often sacrificed during the transfer step. The detailed methodology to calculate the nucleation density is illustrated in Fig. S2. All of the experiments were carried out in described procedures in Fig. 1 in a pressure-controlled CVD system. In this part, we only investigate the depletion stage by fixing other growth parameters such as the flow rate ratio of H_2/CH_4 and the growth time. The carbon embedded in Cu can be depleted by reacting with either H_2 or O_2 gas. The shaded area in. Fig. 1b shows a typical annealing process with H_2 under ~760 Torr for time t_1. After the annealing, CH_4 is introduced into the CVD system to initiate the following refilling and growth from t_1 to t_2. After growth ends, Cu substrate was pulled out of the hot zone and cooled down in a reduced gas atmosphere from t_2 to t_3. With 7 h-long H_2-annealing under high pressure, the average nucleation density reaches ~85 nuclei cm^{-2} (Fig. 1c).

Alternatively, we introduced O_2 to deplete carbon. Fig. 1d displays the growth process with O_2-annealing. The main difference from the H_2-annealing method in Fig. 1b is the CVD system was first vacuumed to ~10 mTorr, in which case the partial pressure of O_2 is equivalent to ~2.5 mTorr. The Cu substrate was moved into the furnace while temperature was ramping up from room temperature to 1070 °C at 50 °C/min. It was stabilized for ~10 min after reaching 1070 °C. The total annealing time of t_1 in Fig. 1b is controlled to be ~0.5 h. By using O_2 as the annealing gas, the average nucleation density drops to ~80 nuclei cm^{-2} (Fig. 1c). The nucleation density is equivalent to that of 7 h H_2-annealing, suggesting a comparable depletion level for these two samples, which will be discussed in following simulation part. When the Cu substrate was intentionally oxidized in the air at 180 °C under ambient pressure for 3 min before being subjected into CVD system, the average nucleation density drops down to ~10 nuclei cm^{-2} (Fig. 1c). All different carbon-depletion experiments were repeated multiple times to make sure their reproducibility. The detailed annealing and growth methods were discussed in Supplementary Information.

2.2. Fabrication and characterization of graphene FET device

The graphene samples on 300 nm thick SiO_2/Si substrates were first located using a scanning electron microscope. The electrodes consisting of Cr/Au (5/25 nm) were deposited with electron-beam lithography, followed with electron-beam evaporation. Oxygen plasma was performed to etch extra graphene with a polymer mask. The graphene FET device was measured using a semiconductor analyzing system (Keithley 4200) at room temperature.

2.3. Optical and spectroscopic measurements

Optical and spectroscopic measurements were characterized using an optical microscopy (Saikedigital 2008L) and a Raman spectroscopy (LabRAM HR, 514 nm laser wavelength).

3. Discussion

The O_2-annealing process leads to a low nucleation density in short time compared to H_2-annealing. Based on this, we propose the carbon diffusion schemes and related mechanisms to describe these two recipes in Fig. 2. The carbon concentration in Cu (C_t) starts from C_s. During the depletion step, it drops down to C_0, which we consider as a thorough depletion status. O_2 (labeled as I) depletes the carbon faster than H_2 (labeled as II). Therefore, plot I has a steeper descending slope than plot II. The carbon refilling steps were using the same rate (H_2/CH_4 = 900:1) in parallel ascending curves. The proposed reacting mechanism of these two processes are shown in Fig. 2b. In the first step of Fig. 2b–I, carbon is gradually depleted from Cu by H_2 during a long annealing time. The possible depletion products could be a series of C_xH_y. The thoroughly depleted Cu with $C_t = C_0$ is obtained. In the next step, CH_4 is introduced into the CVD system and then decomposes into reactive hydrocarbon fragments as the feedstock of carbon atoms. These carbon atoms diffuse from the Cu surfaces into its center. Once C_t reaches C_n, graphene starts to nucleate on Cu surface. The O_2-annealing process is described in Fig. 2b–II. Carbon is reacting with O_2 and depleted from Cu in the form of CO_x. Additional O_2 can also react with Cu and form a copper oxide layer. In the refilling step, the oxide layer gets reduced rapidly with CH_4 and H_2 and carbon atoms start to refill Cu gradually. The graphene nucleates on Cu surface same as Fig. 2b–I once C_t reaches C_n.

To study the refilling conditions, we used thoroughly depleted Cu substrates to carry out two sets of growth experiments: fixed

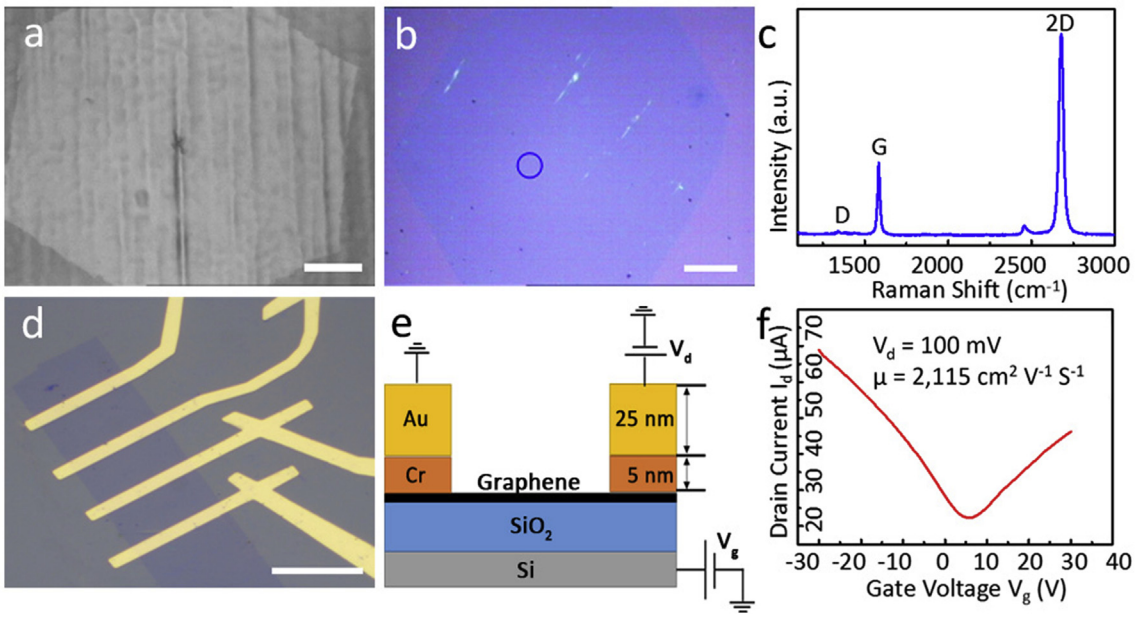

Fig. 4. Characterization of large single crystals synthesized under optimized depletion-refilling condition. (**a**) Representative optical images of graphene single crystals grown under optimized depletion-refilling condition. (**b**) Optical image of the graphene single crystal transferred onto SiO_2/Si substrates. (**c**) Raman spectrum taken from the blue-circled region in (b). (**d**) Optical image of a single crystal graphene FET device on the 300 nm SiO_2/Si substrate. (**e**) The cross sectional structure of a graphene FET. (**f**) Room-temperature electrical transport characterization for the FET device with 100 mV drain voltage. The O_2-annealing times are both 0.5 h and the growth time is 3–5 h. Scale bars: 100 μm in (a), 50 μm in (b), 20 μm in (d). (A colour version of this figure can be viewed online.)

H_2/CH_4 with different growth time (Fig. 3a–d) or different H_2/CH_4 with the same growth time (Fig. 3e–h). We only used O_2-annealing method to deplete the carbon, illustrated by the purple solid lines in Fig. 3a and e. With a H_2/CH_4 ratio of 1280:1, no graphene domains nucleate on Cu within 5 min. As the growth time is stretched to 30 min, very small graphene seed forms (Fig. 3c). Therefore, we can regard 30 min as the fully refilled time under this 1280:1 refilling rate. When the growth time reaches 60 min, these crystals grow slowly in size with an invariable nucleation density ~15 nuclei/cm^2 (Fig. 3d). With H_2/CH_4 of 250:1, the carbon-refilling rate is much faster than the 1280:1 and the nucleation density is too high to be counted, forming a continuous film. With H_2/CH_4 of 600:1, the nucleation density drops to ~110 nuclei/cm^2 (Fig. 3g), and for the H_2/CH_4 is 900:1, it falls further down to ~70 nuclei/cm^2 (Fig. 3h). The carbon refilling process is rather similar to fill an empty pool with water. With longer refilling time and larger carbon flux (lower H_2/CH_4), more carbon atoms can be refilled into Cu. Once the carbon concentration in Cu reaches the saturation point C_n, the refilling ends and nucleation starts.

Via theoretical simulations, we can better understand the behavior of carbon depletion and refilling in Cu. At 1070 °C, the solubility of carbon in Cu is ~10 ppm (Fig. S3) [22]. Although this value is negligible, it indeed plays a critical role in our depletion-refilling-nucleation model. The diffusion coefficient of carbon in Cu is given by D, which is a constant at fixed temperature and its value is $1.78 \times 10^{-7} cm^2 s^{-1}$ at 1070 °C (Supplementary Information Equations (1) and (2)) [23,24].

To study the carbon diffusion behavior in the depletion stage, previous experimental results have shown that 7 h H_2 depletion is similar with 0.5 h O_2 depletion method. It should be noted that the partial pressure difference of the depleting gases has to be taken into account here. We compared the ability of O_2 to deplete carbon with that of H_2 via Fick's law [25]. Results in Fig. S4 and Supplementary Table 1 show that O_2 prevails H_2 in depleting carbon at a rate of ~10^6 times faster. Therefore, the oxidization in air (O_2 pressure ~160 Torr) in Fig. 1d would introduce more oxygen content in Cu, which could further suppress the nucleation centers down to ~10 nuclei cm^{-2}. Throughout the depletion stage, a standard 25-μm-thick Cu substrate keeps a homogenous carbon distribution from center to its surface, with less than 3% concentration variation (Fig. S5). The whole Cu substrate can be taken as "transparent" as the carbon diffusion is kinetically fast enough with its diffusion coefficient ~1.78×10^{-7} $cm^2 s^{-1}$. Thicker Cu substrate means longer route for C to diffuse in and out, which certainly increases the carbon concentration difference between the surface and center of Cu.

In the refilling stage, the direction of C diffusion reverses, going from Cu's carbon-rich surface to its carbon-poor center. This process is analogous to the traditional carburization in iron and steel industry [26]. Our experiment has shown that when H_2/CH_4 is 1280:1, a refilling time of 30 min (Fig. 3c) is needed to saturate the Cu, back from its thoroughly depleted status C_0. The calculated carbon concentration on Cu surface is 10.34 ppm (Supplementary Equation (6)), which is only a little higher than the nucleation concentration C_n, ~10 ppm at growth temperature of 1070 °C. If the refilling time is shorter than 30 min, no detectable graphene seeds form (Fig. 3b). Our simulations also suggest that if H_2/CH_4 is higher than 1335:1, carbon concentration in Cu center would never reach its saturate point, at which the surface carbon concentration is ~10 ppm. Thus no graphene would nucleate on Cu surface. It has been verified by the optical image and Raman data in Fig. S6b, in which we set the H_2/CH_4 as 1500:1 and no graphene nuclei formed on Cu even through the growth time was stretched to 3 h. On the other hand, higher flux of CH_4 gas can saturate the Cu faster (Supplementary Equation (7)). If overflowed carbon sources is given, such as H_2/CH_4 is 250:1, it can saturate the Cu in ~2.5 s. Only 7.8 s is needed for 600:1 and 32.4 s for 900:1, according to our calculation. Although, 2.5 s might be too short in a CVD growth process to be monitored, Fig. S6c shows that graphene can nucleate on Cu in just 25 s when the H_2/CH_4 is 250:1, consistent with our calculations. In this high refilling rate, the nucleation happens too fast to be controlled. For single crystal growth, the flow rate ratio of

H_2/CH_4 between 900:1 and 1280:1 is the most suitable refilling condition. However, for the graphene film growth which doesn't concerns about the nucleation density, the H_2/CH_4 can be set well below 250:1, usually close to ~1:20[6].

By adopting an optimized carbon depletion and refilling method, which is characterized with O_2 annealing for ~0.5 h and a high H_2/CH_4 ratio (900:1), we synthesized graphene single crystals for further electronic measurements. The hexagonal and uniform optical contrast across the crystal suggest only monolayer graphene was synthesized without multilayer seeds and grain boundaries (Fig. 4a–b). The Raman spectrum shows three typical bands, the D (~1350 cm^{-1}), G (~1580 cm^{-1}) and 2D (~2680 cm^{-1}) bands (Fig. 4c). The tiny D band reflects graphene crystal's high quality. The sharp and symmetric 2D bands, with the full width at half maximum (FWHM) of ~33 cm^{-1} and the 2D/G intensity ratio of ~2.69 are consistent with the Raman signatures of single layer graphene [27,28]. We also fabricated the field effect transistor (FET) devices from this graphene sample to evaluate its electrical property (see Methods). Fig. 4d displays the optical microcopy image of the FET device made from a single-crystal graphene and Fig. 4e represents the cross section layout of the device. The electron mobility (μ) is ~2115 $cm^2\ V^{-1}\ S^{-1}$ calculated from the data presented in Fig. 4f, comparable with the best CVD graphene samples [29–31]. The detailed electrical transport calculation is in the Supplementary Information Equations (8) and (9).

4. Conclusions

In summary, we have systematically studied the CVD graphene growth and nucleation behavior in O_2 or H_2 annealing environments, and proposed a carbon-depletion-refilling mechanism. According to this mechanism, we can readily calculate the carbon depletion and refilling rate for different graphene growth systems, and optimize the outcomes with both low nucleation density and high repeatability. Theoretical simulations reveal that O_2 can deplete the carbon in Cu ~10^6 times faster than H_2. With additional oxidation at 180 °C in air, the nucleation density further drops down to ~10 nuclei cm^{-2} in half an hour. This illuminates a promising path for CVD graphene's scale-up production, in an efficient and standard way. On the other hand, the growth speed is another important issue in graphene's mass production, which is definitely worth pursuing in future studies.

Acknowledgements

This work was financially supported by the National Natural Science Foundation of China (21301032), National Key Research and Development Program of China (2016YFA0203900).

Appendix A. Supplementary data

Supplementary data related to this article can be found at http://dx.doi.org/10.1016/j.carbon.2017.04.055.

References

[1] X.S. Li, et al., Transfer of large-area graphene films for high-performance transparent conductive electrodes, Nano Lett. 9 (12) (2009) 4359–4363, http://dx.doi.org/10.1021/nl902623y.
[2] A.H. Castro Neto, F. Guinea, N.M.R. Peres, K.S. Novoselov, A.K. Geim, The electronic properties of graphene, Rev. Mod. Phys. 81 (2009) 109, http://dx.doi.org/10.1103/RevModPhys.81.109.
[3] D.S.L. Abergel, V. Apalkov, J. Berashevich, K. Ziegler, T. Chakraborty, Properties of graphene: a theoretical perspective, Adv. Phys. 59 (4) (2010) 261.
[4] X. Huang, et al., Graphene-based materials: synthesis, characterization, properties, and applications, Small 7 (14) (2011) 1876–1902, http://dx.doi.org/10.1002/smll.201002009.
[5] A.A. Balandin, et al., Superior thermal conductivity of single-layer graphene, Nano Lett. 8 (3) (2008) 902–907, http://dx.doi.org/10.1021/nl0731872.
[6] X.S. Li, et al., Large-area synthesis of high-quality and uniform graphene films on copper foils, Science 324 (5932) (2009) 1312–1314, http://dx.doi.org/10.1126/science.1171245.
[7] X.S. Li, et al., Graphene films with large domain size by a two-step chemical vapor deposition process, Nano Lett. 10 (11) (2010) 4328–4334, http://dx.doi.org/10.1021/nl101629g.
[8] A. Reina, et al., Large area, few-layer graphene films on arbitrary substrates by chemical vapor deposition, Nano Lett. 9 (1) (2009) 30–35, http://dx.doi.org/10.1021/nl801827v.
[9] S. Bae, et al., Roll-to-roll production of 30-inch graphene films for transparent electrodes, Nat. Nanotechnol. 5 (2010) 574–578, http://dx.doi.org/10.1038/nnano.2010.132.
[10] D. Wei, Y. Liu, Controllable synthesis of graphene and its applications, Adv. Mater. 22 (30) (2010) 3225–3241, http://dx.doi.org/10.1002/adma.200904144.
[11] W. Wu, et al., Growth of single crystal graphene arrays by locally controlling nucleation on polycrystalline Cu using chemical vapor deposition, Adv. Mater. 23 (42) (2011) 4898–4903, http://dx.doi.org/10.1002/adma.201102456.
[12] A.W. Robertson, J.H. Warner, Hexagonal single crystal domains of few-layer graphene on copper foils, Nano Lett. 11 (3) (2011) 1182–1189, http://dx.doi.org/10.1021/nl104142k.
[13] I. Vlassiouk, et al., Role of hydrogen in chemical vapor deposition growth of large single-crystal graphene, ACS Nano 5 (7) (2011) 6069–6076, http://dx.doi.org/10.1021/nn201978y.
[14] Z.Z. Sun, et al., Growth of graphene from solid carbon sources, Nature 468 (2010) 549–552, http://dx.doi.org/10.1038/nature09579.
[15] Y.A. Wu, et al., Large single crystals of graphene on melted copper using chemical vapor deposition, ACS Nano 6 (6) (2012) 5010–5017, http://dx.doi.org/10.1021/nn3016629.
[16] D. Geng, et al., Uniform hexagonal graphene flakes and films grown on liquid copper surface, Proc. Natl. Acad. Sci. U.S.A. 109 (21) (2012) 7992–7996, http://dx.doi.org/10.1073/pnas.1200339109.
[17] H.L. Zhou, et al., Chemical vapour deposition growth of large single crystals of monolayer and bilayer graphene, Nat. Commun. 4 (2013) 2096.
[18] Z. Yan, Z.W. Peng, James M. Tour, Chemical vapor deposition of graphene single crystals, Acc. Chem. Res. 47 (4) (2014) 1327–1337, http://dx.doi.org/10.1021/ar4003043.
[19] S.S. Chen, et al., Millimeter-size single-crystal graphene by suppressing evaporative loss of Cu during low pressure chemical vapor deposition, Adv. Mater. 25 (14) (2013) 2062–2065, http://dx.doi.org/10.1002/adma.201204000.
[20] J. Li, et al., Facile growth of centimeter-sized single-crystal graphene on copper foil at atmospheric pressure, J. Mater. Chem. C 3 (15) (2015) 3530–3535.
[21] T.R. Wu, et al., Fast growth of inch-sized single-crystalline graphene from a controlled single nucleus on Cu–Ni alloys, Nat. Mater. 15 (2016) 43–47, http://dx.doi.org/10.1038/nmat4477.
[22] G.A. Lopez, E.J. Mittemeijer, The solubility of C in solid Cu, Scr. Mater. 51 (1) (2004) 1–5, http://dx.doi.org/10.1016/j.scriptamat.2004.03.028.
[23] R. Abbaschian, L. Abbaschian, R.E. Reed-Hill, Physical Metallurgy Principles, 4th ed., Cengage learning Press, Stamford, CT, 2009, pp. 262–350.
[24] Y.F. Hao, et al., Oxygen-activated growth and bandgap tenability of large single-crystal bilayer graphene, Nat. Nanotechnol. 11 (2016) 426–431, http://dx.doi.org/10.1038/nnano.2015.322.
[25] X.L. Song, X.H. Huang, Fundamentals of Inorganic Materials Science, Chemical Industry Publishing House, Beijing, 2006, pp. 301–310.
[26] G.G. Tibbetts, Diffusivity of carbon in iron and steels at high temperatures, J. Appl. Phys. 51 (1980) 4813–4816, http://dx.doi.org/10.1063/1.328314.
[27] A.C. Ferrari, D.M. Basko, Raman spectroscopy as a versatile tool for studying the properties of graphene, Nat. Nanotechnol. 8 (2013) 235–246, http://dx.doi.org/10.1038/nnano.2013.46.
[28] A.C. Ferrari, et al., Raman spectrum of graphene and graphene layers, Phys. Rev. Lett. 97 (18) (2006) 187401.
[29] F. Schwierz, Graphene transistor, Nat. Nanotechnol. 5 (2010) 487–496, http://dx.doi.org/10.1038/nnano.2010.89.
[30] B. Radisavljevic, A. Radenovic, J. Brivio, V. Giacometti, A. Kis, Single-layer MoS_2 transistor, Nat. Nanotechnol. 6 (2011) 147–150, http://dx.doi.org/10.1038/nnano.2010.279.
[31] G.Y. Lu, et al., Synthesis of large single-crystal hexagonal boron nitride grains on Cu–Ni alloy, Nat. Commun. 6 (2015) 6160.